Prediction models for assessing anthocyanins in grape berries by fluorescence sensors: Dependence on cultivar, site and growing season

Patrizia Pinelli[a,*], Annalisa Romani[a], Elisa Fierini[a], Giovanni Agati[b]

[a] DiSIA – Department of Statistics, Computer Sciences and Applications – PHYTOLAB Laboratory, Scientific and Technological Pole, University of Florence, Via Ugo Schiff, 6, 50019 Sesto Fiorentino, Firenze, Italy
[b] Istituto di Fisica Applicata "Nello Carrara" IFAC, Consiglio Nazionale delle Ricerche, Via Madonna del Piano 10, 50019 Sesto Fiorentino, Firenze, Italy

ARTICLE INFO

ABSTRACT

Fluorescence sensors are useful tools for the non-destructive assessment of grape berry anthocyanins. The Multiplex (Mx) sensor here studied provides two anthocyanin indices: $ANTH_R = \log(1/Chl\text{-}fluorescence\_R)$ and $ANTH_{RG} = \log(Chl\text{-}fluorescence\_R/Chl\text{-}fluorescence\_G)$, based on the chlorophyll (Chl) fluorescence excited with red (R) and green (G) light. These indices were calibrated against wet chemistry. The dependence of anthocyanin prediction models on cultivar, season and site was studied on four cultivars in two Italian regions during three consecutive years. The 2010 global model (all cultivars at both growing sites) gave relative prediction errors on anthocyanin content less than 14.1% ($ANTH_R$) and 19.0% ($ANTH_{RG}$). The $ANTH_{RG}$ was independent of season, maintaining a relative error of about 20% in both 2011 and 2012. In field applications of the calibrated Mx, it showed its ability to detect inter-plot and inter-season differences on both growing sites.

1. Introduction

It is now well accepted that a premium wine trait depends on the quality of the grapes used to produce it, and an important parameter that lends credibility to this premise is the colour of the wine. Anthocyanins (Anths), the red pigments of the berry skins that define the colour of wines, are good indicators of the so-called phenolic maturity of grapes. Phenolic maturity can be assessed by measuring either total phenolics or skin anthocyanin content, which is closely correlated with total phenolics (Kennedy, Matthews, & Waterhouse, 2002). In most red grape varieties, Anths are located in the berry skin and accumulate, starting from véraison, until the grapes ripen fully (Boss, Davies, & Robinson, 1996). In addition to technological maturity, i. e. the acidity and sugar content of berries, phenolic maturity has now become the main concern of viticulturists and oenologists in planning harvest time and in choosing the most appropriate oenological techniques. Therefore, an accurate determination of the Anth content in the berries is fundamental.

This is routinely performed by using destructive 'wet chemistry' procedures, which are costly and time-consuming. Conversely, the non-destructive evaluation of the optical sensors can be extremely advantageous on the large biological variability of grape-berry Anths. In fact, a large number of samplings representative of the whole crop can be measured directly in the vineyard within relatively short time periods. Furthermore, the maturity process can also be followed on the same bunches during the entire season, by repeating the optical measurements at a high frequency. For this purpose, the Multiplex® sensor (FORCE-A, Orsay, France), a no-contact, hand-held optical device, has been developed (Cerovic et al., 2008). It measures Anths in an indirect way that is based on the interference effect exerted by anthocyanin absorbance over chlorophyll fluorescence excitation in the green and red spectral regions (Agati, Meyer, Matteini, & Cerovic, 2007). The sensor provides two Anth indices: the $ANTH_R$ based on a single signal, the far-red chlorophyll fluorescence under red excitation, also called the FERARI (Fluorescence Excitation Ratio Anthocyanin Relative Index) index (Ben Ghozlen, Cerovic, Germain, Toutain, & Latouche, 2010) and the $ANTH_{RG}$ based on two signals, i.e. the ratio between far-red chlorophyll fluorescence under both red and green excitation.

Several applications of the Multiplex (Mx) sensor directly in the vineyards, for the manual determination of Anth evolution in a large

---

number of bunches, have been reported (Baluja, Diago, Goovaerts, & Tardaguila, 2012a; Ben Ghozlen et al., 2010; Tuccio et al., 2011). It has been used for assessing the spatial variability of grape colour and for correlating this to several agronomic parameters, such as vine vigour and yield (Baluja, Diago, Goovaerts, & Tardaguila, 2012b).

The use of Mx as an on-the-go sensor mounted on a harvester has also been demonstrated (Bramley et al., 2011). Besides determining Anth, the Mx acts as a tool for characterizing the spatial variability of the vegetative status of the vineyard (Diago et al., 2016).

The Mx sensor can also represent a useful device for the winery laboratories as an alternative to UV–Vis spectroscopy colourimetric analyses of grape berries. In fact, there is a growing interest in adopting non-destructive techniques for the evaluation of grape quality, such as NIR hyperspectral imaging coupled with chemometrics (Chen et al., 2015; Nogales-Bueno, Baca-Bocanegra, Rodríguez-Pulido, Heredia, & Hernández-Hierro, 2015; Zhang et al., 2017).

In general, any sensor aimed at being correctly quantitative must be calibrated against chemical determinations of the target molecules.

Previous studies have reported several calibrations of the Mx for Anth estimation in grape berries (Agati et al., 2013; Baluja et al., 2012a; Ben Ghozlen et al., 2010; Bramley et al., 2011; Ferrandino et al., 2017; Tuccio et al., 2011). The Anth levels investigated ranged from 0.7 to 0.8 mg g^{-1} in Pinot Noir, Pinot Menier, Aleatico and Nebbiolo to about 2 mg g^{-1} in Tempranillo, Merlot and Barbera, and up to 2.5 mg g^{-1} in Shiraz and Cabernet Sauvignon. These prediction models were obtained from single-year determinations and differed as a function of the cultivar. Ferrandino et al. (2017) also reported on the dependence of ANTH$_{RG}$ on the cultivar Anth profile.

The morphological differences among grape varieties in size, weight and berry-skin thickness may have a dissimilar influence on the optical signals acquired by the Mx. Significant differences may also occur for the same variety from one winery to another, as they are influenced both by the terroir and by the different cultural practices. Variability among seasons in the meteorological conditions, particularly temperature and dryness, can induce water stress status in the vines, thus affecting berry size and Anth synthesis (Deluc et al., 2009; Ojeda, Andary, Kraeva, Carbonneau, & Deloire, 2002; Tuccio et al., 2011).

For this reason, an evaluation of both the cultivar and the environmental and growing-place effects on the Mx calibration is required. In this paper, the berry anthocyanin concentrations have been correlated with the Mx indices (ANTH$_R$ and ANTH$_{RG}$) in order to build different calibration models for i) individual cultivars, ii) the same cultivar in two different regions, iii) three cultivars on one site and, lastly, iv) all cultivars on two sites. The seasonal robustness of the models was evaluated by means of validation over three successive years. The Mx calibration models defined were then used to estimate Anth non-destructively from in-vineyard Mx measurements. Examples of applications concerning the comparison of Anth among different plots and years of the same cultivar per site, the comparison of Anth for the same cultivar between different sites and years, and the temporal evolution of Anth have also been reported.

2. Material and methods

2.1. Plant material and growing sites

The experiment was conducted over three consecutive years (2010–2012) at the Casale del Giglio (Aprilia, LT, Italy; 41°30′44.0″N, 12°44′44.2″E) and Castello Banfi (Montalcino, SI, Italy; 42°58′49.22″N, 11°23′55.59″E) wine estates. Casale del Giglio (CdG) is located in the Agro-Pontino Valley, 10 km from the Tyrrhenian Sea coast on a flat area (0–20 m of elevation) that is characterized by a maritime climate. Three cultivars from among the 160 ha of vineyards cultivated at CdG – namely, Merlot (ME), Petit Verdot (PV) and Syrah (SH) – were considered. The three varieties were bred using the Guyot or spur-pruned cordon system and the vines spaced 2.2 m × 0.8 m (inter- and intra-

row). Two to three plots, which differed as regards clones and soil texture, were selected for each variety: 3A and 20 for Merlot, 30, 7 and 1B for Petit Verdot, and 2B, 6 and 21B for Syrah.

At the Castello Banfi (CB) estate, located in a territory that occupies 2830 ha, 850 ha of which are for specialized vineyards, three red varieties and two to three plots per cultivar were considered. In particular: plots 23.04, 37.05 and 7.04 for cv. Merlot (ME), plots 12.07 and 10.13 for cv. Syrah (SH), and plots 24.09 and 7.03 for cv. Cabernet Sauvignon (CS). The three varieties were bred using the low spur-pruned cordon system and the vines were spaced 3.0 m × 0.8 m (inter- and intra- row). CB is located on an inner hillside (200–600 m a.s.l.) in southern Tuscany. The entire area is characterized by a temperate climate, with high exposure to the sun and to breezes and considerable variations between daytime and night-time temperatures.

The climatic conditions, global radiation, air temperature and rainfall recorded in the two regions during the 2010–2012 seasons are reported as online Supplementary materials (Fig. S1 and Table S1). The heat accumulation index for *Vitis vinifera* L., that is, the growing degree-days (GDD) index, was calculated according to Winkler (1974).

2.2. Optical sensor and indices

The Multiplex® (Mx) fluorimetric sensor (FORCE-A, Orsay, France) is described in detail elsewhere (Ben Ghozlen et al., 2010). It measures fluorescence emitted by chlorophyll in the 670–690 nm red (RF) and 720–780 nm far-red (FRF) spectral regions, under excitation with different light-emitting diode (LED) sources in the UV (375 nm) and visible (blue at 450 nm, green at 515 nm and red at 630 nm). Since the LED sources are pulsed and synchronized with the detection, the sensor is insensitive to ambient light and can be used directly in the vineyard. The wide detection area of the sensor (8-cm diameter) makes it possible for a signal to be acquired from a large area in each bunch. The acquisition time for a single bunch sample is less than 1 s. The collected data, which are visible on a real-time display, are stored on a secure digital card for data elaboration.

The fluorescence indices used in this work are defined as:

$$ANTH_{RG} = \log(FRF_R/FRF_G) \tag{1}$$

$$ANTH_R = \log(1/FRF_R) \tag{2}$$

where FRF$_R$ and FRF$_G$ are the far-red chlorophyll fluorescence signals excited by red and green light, respectively (Ben Ghozlen et al., 2010). Signals were corrected for residual electronic offsets and normalized to a fluorescence standard (blue plastic foil, FORCE-A, Orsay, France).

The selected bunches were extracted and analysed in the laboratory by means of spectrophotometric analysis, in order to evaluate the anthocyanin content. These data were then used to calibrate and validate the Mx optical sensor, as described here as follows.

2.3. Sampling for calibration and in field measurements

Samples of grapes were collected at different stages of ripening, from green to véraison until full ripeness, in order to cover as broad as possible a range of Anths content.

At CdG, the sampling dates were 20 and 26 August, 2, 9, 16 and 23 September for the 2010 campaign, 24 and 31 August, 8 and 14 September for the 2011 campaign, and 23 and 30 August, 12 September for the 2012 campaign. At CB, the sampling dates were 17 and 31 August, 10, 20 and 27 September, 5 and 12 October for the 2010 campaign; 29 August, 6, 12 and 21 September for the 2011 campaign; and 29 August and 11 September for the 2012 campaign.

The samples collected (2–3 bunches) were transported under cool conditions to the laboratory for further analysis.

On the same dates of sampling, in-field Mx measurements on bunches attached to the vines were performed as follows. At the beginning of the 2010 campaign, 2–4 rows per plot, depending on the plot size,

were selected and marked. Twenty-five bunches per row were measured by the Mx, and the very same portion of each row was monitored over time until the harvest. The same rows of the same plots were also measured during the 2011 season.

2.4. Calibration of fluorescence indices against wet chemistry

From each single cultivar sample collected in the field, 19 berries (i.e. those filling the $5 \times 10^3 \, mm^2$ circular area of the sensor window) were selected and placed on a special support to simulate their position in the grape bunch, oriented with the apical side upwards (see Fig. S2 in the Supplementary material). They were then measured with the sensor at a fixed distance.

After being measured, each 19 berry-sample was weighed, homogenized in a blender for 20 s and, then, extracted and analysed. In particular, a quantity of 5 g of the homogenate was extracted 1 h at room temperature by 50 mL of hydroalcoholic solution (70% ethanol and 30% Milli Q water acidified at pH 1.4 by HCl). The extract was measured by means of the spectrophotometer Cary 50 (Agilent Technologies, Santa Clara, CA) that was provided with an optical fibre, after being filtered and diluted. The sample absorbance was measured at 520 nm. Total Anths were expressed as malvidin-3-*O*-glucoside or oenin ($\varepsilon_{520} = 16,101 \, Lcm^{-1}mol^{-1}$), using a calibration curve of five levels of concentration ($R^2 > 0.998$). The resulting data were used to calibrate and validate both $ANTH_R$ and $ANTH_{RG}$ indices of the Mx optical sensor.

For each data set, calibration curves were built to fit the scatter plot between the anthocyanin concentrations determined by wet chemistry and the corresponding Mx fluorescence anthocyanin indices determined in the laboratory by means of the Mx.

The Anth concentration was expressed per berry mass ($Anth_g$), i.e. milligrams of Anth per grams of berry fresh weight, since it is the main unit used in winery laboratories. However, some considerations on $Anth_m$, the Anth concentration per berry skin mass, for an interpretation of seasonal effects on the calibration models are also presented. In particular, $Anth_g$ was the parameter directly measured by means of berry extraction and spectrophotometric determination, while $Anth_m$ was calculated by using the berry mass and the CUBA (Converter of Units of Berry Anths) software (Cerovic et al., 2014).

By following this procedure from the data collected during the 2010–2012 campaigns, different calibration curves (as previously described) were calculated and compared. The data were processed using the SigmaPlot 12.5 programme (SYSTAT software, Inc. SigmaPlot for Windows).

2.5. Calibration for in field application

As observed previously (Ben Ghozlen et al., 2010; Bramley et al., 2011), the Anth Mx indices measured on a bunch of grapes were shifted as compared with those measured on berries from the same bunch detached and arranged in a cluster-like holder, as described above. The reason for this is not yet known, but it is most likely due to a geometrical effect that can change the amount of berry-scattered light collected by the sensor in the two different configurations. However, by comparing bunch measurements in the field with berry measurements of sampling from the same sub-plot, a fine correlation between the two sets of Anth indices was found (see data reported in Fig. S3 of Supplementary material). This correlation was considered in order to convert the calibration curves built with the optical measurements in the laboratory into those to be used in the field.

2.6. Solvents and chemicals

Water was purified with the use of a Milli-Q system (Bedford, MA, USA). The ethanol and hydrochloric acid used for the grape extractions were supplied by Sigma-Aldrich. The authentic standard of malvidin 3-

O-β-D-glucoside or oenin (> 90% HPLC) was purchased from Extrasynthese (Nord Genay, Lyon, France).

2.7. Statistical analysis

Statistical analysis was carried out using the SigmaPlot Program 12.5 (Systat Software, Inc. SigmaPlot for Windows), and statistical differences were evaluated by means of t-test analysis or by the all-pairwise, multiple-comparison Tukey ANOVA test. P values of < 0.05 were considered statistically significant. The accuracy of the calibration curves was described by the Root Mean Square Error of Calibration (RMSEC) and the coefficient of determination (R^2). The Root Mean Square Error of Prediction (RMSEP) was calculated in order to evaluate the predictive ability of the regression models. The Relative Error (RE) was defined as the percentage of RMSEP relative to the mean Anth values measured at harvest (calculated over the last 2 weeks before harvest), in order to compare the model performances with each other.

Each data set was sorted into increasing Anth values and then divided, from the minimum to the maximum, into categories of 3–4 data each. From each category, one value was randomly chosen to define the validation data set corresponding to one-third of the entire data. The remaining two-thirds were used as a calibration data set. This way ensured that the whole range of Anth was covered both in the calibration and validation data sets. The procedure was repeated five times; the average values ($\pm$ SD) of R^2 and RMSEC for the models of calibration and the RMSEP and RE for the model validation were then calculated.

3. Results and discussion

3.1. Calibration models

In order to define a robust calibration of the Mx sensor for evaluating the Anth content of the grape berries, a heterogeneous set of data obtained from various cultivars and from two different geographical regions was employed.

3.1.1. Individual cultivars per site

Fig. 1 shows the relationship between the Mx indices and the total anthocyanin content per berry mass ($Anth_g$) of sampling collected for all the cvs and the two investigated sites during the entire 2010 season. All points of each data set were registered during and after véraison.

As expected on the basis of previous studies, the $ANTH_R$ was positively correlated to $Anth_g$ over the entire range of data and for all cultivars. The calibration curve derived for $ANTH_R$ was represented in any case by a homographic function, with $R^2 > 0.9$ (see data reported in Table S2 of Supplementary materials).

$ANTH_{RG}$ increased up to a maximum with an increase in the $Anth_g$ during véraison, and then showed an opposite trend from complete véraison to harvest time. This bi-phasic behaviour, as previously reported (Ben Ghozlen et al., 2010), can be understood considering that $ANTH_{RG}$ is given, by definition (Eq. (1)), by the difference between $logFRF_R$ and $logFRF_G$. Both these two components decrease exponentially with increasing $Anth_g$, being inverse functions of the Anth absorbance. However, the component in the green decreases faster than that in the red, because of the larger absorbance of Anth at green wavelengths. The resulting curve representing the $ANTH_{RG}$ versus the $Anth_g$ relationship is that depicted in Fig. 1 with the use of dotted lines. Calibration of the $ANTH_{RG}$ can be problematic, since the bi-exponential function cannot be inverted analytically and even a numerical solution to it can cause ambiguity around véraison or at lower $Anth_g$ values. It was therefore suggested to use the $ANTH_{RG}$ index only when véraison had been completed (Bramley et al., 2011). For all cvs, the calibration curves derived for $ANTH_{RG}$, when considering only post-véraison data (closed triangles in Fig. 1), were represented by an exponential decaying function. In all cases except cv. CS ($R^2 = 0.543$), at least 80% of
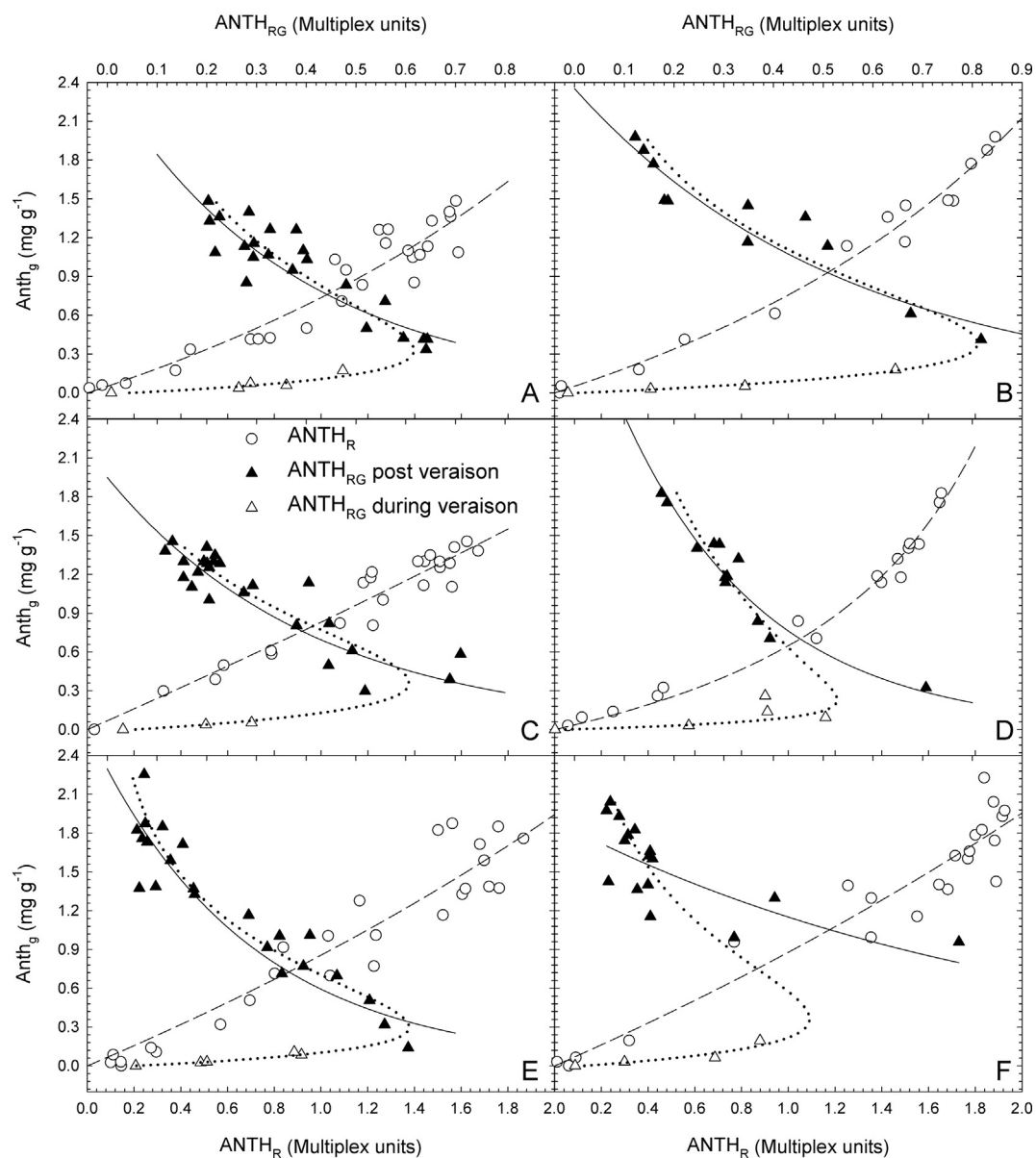
Fig. 1. Multiplex calibration curves for individual cultivars. The scatter plots of Anth$_g$ versus ANTH$_R$ are described by homographic functions y = x/(a + bx) (see Table S2 of Supplementary material for fitting parameters); the scatter plots of Anth$_g$ versus ANTH$_{RG}$ post veraison are described by exponential functions y = ae^{-bx} (see Table S2 of Supplementary material for fitting parameters). Cultivars grown at Casale del Giglio: SH (A), ME (C) and PV (E). Cultivars grown at Castello Banfi: SH (B), ME (D) and CS (F).

the Anth$_g$ versus ANTH$_{RG}$ distribution was explained by the exponential function (see data reported in Table S2 of Supplementary materials). Significant differences appeared in the ME calibration curves for both indices between the two sites (Fig. 1C and D and Table S2), while SH calibration curves at CdG and CB were rather similar (Fig. 1A and B and Table S2).

The lowest RMSEC (0.075 mg g^{-1}) was found for ANTH$_R$ in ME at CB, while the highest (0.229 mg g^{-1}) was obtained for ANTH$_{RG}$ in PV at CdG. A better comparison of the model performances can be obtained by considering the RMSEP and RE values from the cross-validation process reported in Tables 1 and 2, as averages of five repetitions. For both Mx indices, the calibration curves built with 2/3 of the data were comparable to those built with the entire set of data in terms of R^2 and RMSEC (compare values in Tables 1 and 2 with those in Table S2). By using ANTH$_R$, the best model for Anth$_g$ prediction was obtained for SH at CB (RE = 7.4%) and the highest RE was recorded for SH at CdG (13.4%) (Table 1). The ANTH$_{RG}$ model produced higher RE than the ANTH$_R$ one, ranging from 8.7% (ME at CB) to 16% (SH at CB).

3.1.2. Inter-site for individual cultivars

For the two cvs present on both the CdG and CB estates, i.e. Shiraz and Merlot, an inter-site calibration model was considered, using the single cv data from the two sites. The calibration curves obtained were validated on the same data set considered for the validation of the previous single-cv single-site models. The results of this analysis are reported in Tables 1 and 2, for ANTH$_R$ and ANTH$_{RG}$, respectively. The inter-site ANTH$_R$ calibration model was very similar to that of the individual cvs (compare R^2 and RMSEC between the first two rows for SH and ME in Table 1).

The percentage relative error was less than 13.5%, close to and sometimes even better than the values obtained from the single-site calibration models.

On the whole, no significant differences were observed (P value > 0.05) between the inter-site models and the single-cv models.

When considering the inter-site ANTH$_{RG}$ models, it was found that the calibration parameters were similar to those of the single-site ones (Table 2). However, the differences between the two models were

Table 1
Calibration (R^2 and RMSEC) and validation (relative error, RE and RMSEP) parameters of different calibration models for the $ANTH_R$ index against $Anth_g$: i) individual cultivar, ii) one cultivar at two sites, iii) all the cultivars at one site, iv) global curve (all the cultivars at both sites).

Site/Cultivar	RMSEP (mg g^{-1})	Validation		Data set	Calibration		No. of samples
		RE (%)	No. of samples		R^2	RMSEC (mg g^{-1})	
CdG							
SH	0.165 ± 0.017	13.4 ± 1.3	9	SH[i]	0.921 ± 0.009	0.140 ± 0.008	18
	0.165 ± 0.022	13.5 ± 1.7		SH CdG + CB[ii]	0.956 ± 0.006	0.123 ± 0.009	28
	0.164 ± 0.021	13.4 ± 1.6		SH + ME + PV CdG[iii]	0.916 ± 0.016	0.155 ± 0.024	53
	0.172 ± 0.029	14.1 ± 2.3		Global[iv]	0.929 ± 0.004	0.164 ± 0.005	90
ME	0.109 ± 0.024	8.2 ± 1.8	8	ME[i]	0.951 ± 0.012	0.109 ± 0.012	17
	0.119 ± 0.034	9.0 ± 2.4		ME Cdg + CB[ii]	0.953 ± 0.006	0.120 ± 0.008	29
	0.109 ± 0.020	8.2 ± 1.4		SH + ME + PV CdG[iii]	0.916 ± 0.016	0.155 ± 0.024	53
	0.114 ± 0.029	8.7 ± 2.1		Global[iv]	0.929 ± 0.004	0.164 ± 0.005	90
PV	0.178 ± 0.042	10.3 ± 2.3	8	PV[i]	0.893 ± 0.014	0.221 ± 0.015	18
	0.176 ± 0.044	10.2 ± 2.5		SH + ME + PV CdG[iii]	0.916 ± 0.016	0.155 ± 0.024	53
	0.176 ± 0.039	10.2 ± 2.2		Global[iv]	0.929 ± 0.004	0.164 ± 0.005	90
CB							
SH	0.113 ± 0.026	7.4 ± 1.8	5	SH[i]	0.985 ± 0.004	0.092 ± 0.013	10
	0.107 ± 0.014	6.3 ± 0.8		SH CdG + CB[ii]	0.956 ± 0.006	0.123 ± 0.009	28
	0.090 ± 0.036	5.9 ± 2.4		SH + ME + CS CB[iii]	0.944 ± 0.008	0.162 ± 0.013	37
	0.094 ± 0.029	6.2 ± 1.9		Global[iv]	0.929 ± 0.004	0.164 ± 0.005	90
ME	0.108 ± 0.010	7.8 ± 1.0	5	ME[i]	0.991 ± 0.002	0.065 ± 0.006	12
	0.101 ± 0.075	7.1 ± 5.1		ME Cdg + CB[ii]	0.953 ± 0.006	0.120 ± 0.008	29
	0.108 ± 0.065	7.6 ± 4.4		SH + ME + CS CB[iii]	0.944 ± 0.008	0.162 ± 0.013	37
	0.100 ± 0.066	7.0 ± 4.4		Global[iv]	0.929 ± 0.004	0.164 ± 0.005	90
CS	0.190 ± 0.067	11.3 ± 4.1	7	CS[i]	0.890 ± 0.022	0.218 ± 0.025	15
	0.166 ± 0.062	9.9 ± 3.8		SH + ME + CS CB[iii]	0.944 ± 0.008	0.162 ± 0.013	37
	0.159 ± 0.057	9.5 ± 3.5		Global[iv]	0.929 ± 0.004	0.164 ± 0.005	90

significant ($P < 0.001$) only for ME at CB, with R^2 reduced from 0.92 to 0.78 and RMSEC, RMSEP and RE almost doubled. In all the other cases, SH at CdG and CB and ME at CdG, no significant differences were observed.

3.1.3. Inter-cultivar per site

Here, inter-cultivar calibration models for each of the two regions, i.e. SH, ME and PV at CdG and SH, ME and CS at CB, were considered. For $ANTH_R$ models, again no statistically significant ($P > 0.05$) variations were found in the calibration and validation parameters as

Table 2
Calibration (R^2 and RMSEC) and validation (relative error, RE and RMSEP) parameters of different calibration models for the $ANTH_{RG}$ index against $Anth_g$: i) individual cultivar, ii) one cultivar at two sites, iii) all the cultivars at one site, iv) global curve (all the cultivars at both sites).

Site/Cultivar	RMSEP (mg g^{-1})	Validation		Data set	Calibration		No. of samples
		RE (%)	No. of samples		R^2	RMSEC (mg g^{-1})	
CdG							
SH	0.192 ± 0.027	16.0 ± 2.1	7	SH[i]	0.846 ± 0.018	0.177 ± 0.011	14
	0.174 ± 0.021	13.9 ± 1.8		SH CdG + CB[ii]	0.797 ± 0.026	0.220 ± 0.008	22
	0.230 ± 0.050	19.2 ± 4.0		SH + ME + PV CdG[iii]	0.836 ± 0.016	0.210 ± 0.025	46
	0.191 ± 0.033	14.4 ± 2.2		Global[iv]	0.784 ± 0.019	0.242 ± 0.017	72
ME	0.159 ± 0.032	12.3 ± 2.6	8	ME[i]	0.830 ± 0.045	0.183 ± 0.038	16
	0.164 ± 0.025	12.7 ± 2.0		ME Cdg + CB[ii]	0.781 ± 0.040	0.213 ± 0.022	24
	0.164 ± 0.019	12.6 ± 1.6		SH + ME + PV CdG[iii]	0.836 ± 0.016	0.210 ± 0.025	46
	0.174 ± 0.017	12.9 ± 1.2		Global[iv]	0.784 ± 0.019	0.242 ± 0.017	72
PV	0.190 ± 0.030	10.3 ± 1.2	7	PV[i]	0.884 ± 0.004	0.234 ± 0.031	14
	0.166 ± 0.061	8.9 ± 3.0		SH + ME + PV CdG[iii]	0.836 ± 0.016	0.210 ± 0.025	46
	0.165 ± 0.072	8.9 ± 3.6		Global[iv]	0.784 ± 0.019	0.242 ± 0.017	72
CB							
SH	0.164 ± 0.031	9.6 ± 2.0	4	SH[i]	0.897 ± 0.022	0.184 ± 0.023	7
	0.240 ± 0.080	14.0 ± 4.7		SH CdG + CB[ii]	0.797 ± 0.026	0.220 ± 0.008	22
	0.211 ± 0.036	12.3 ± 2.1		SH + ME + CS CB[iii]	0.758 ± 0.077	0.224 ± 0.092	26
	0.328 ± 0.065	19.0 ± 3.9		Global[iv]	0.784 ± 0.019	0.242 ± 0.017	72
ME	0.133 ± 0.026	8.7 ± 2.3	4	ME[i]	0.923 ± 0.059	0.122 ± 0.021	8
	0.294 ± 0.012	19.0 ± 1.5		ME Cdg + CB[ii]	0.781 ± 0.040	0.213 ± 0.022	24
	0.218 ± 0.019	14.1 ± 1.3		SH + ME + CS CB[iii]	0.758 ± 0.077	0.224 ± 0.092	26
	0.267 ± 0.021	17.3 ± 1.9		Global[iv]	0.784 ± 0.019	0.242 ± 0.017	72
CS	0.243 ± 0.021	13.1 ± 0.8	5	CS[i]	0.602 ± 0.045	0.199 ± 0.007	11
	0.221 ± 0.051	12.4 ± 2.8		SH + ME + CS CB[iii]	0.758 ± 0.077	0.224 ± 0.092	26
	0.200 ± 0.061	11.3 ± 3.4		Global[iv]	0.784 ± 0.019	0.242 ± 0.017	72

compared with the individual cv models (Table 1). The trend was slightly worse for SH and ME at both sites, but was better for PV and CS. These data suggested that for the three cvs investigated, a sufficient accuracy in the $Anth_g$ prediction could be obtained in the same geographical area by using a single inter-cv model.

The same conclusion could be drawn for the $ANTH_{RG}$ models, with the sole exception of ME at CB, for which the RE of 14.1% given by the inter-cv calibration was significantly (P = 0.006) higher than that from the individual-cv model (8.7%) (see Table 2).

3.1.4. Global (inter-cultivar and inter-site) calibration models

Lastly, an evaluation was performed of global calibration models that included all the cvs at both sites. The comparison of these models with the individual-cv models led to the same conclusion as before. The accuracy of prediction was essentially the same for the two models, with the exception of the $ANTH_{RG}$ relative to SH and ME at CB, the global model for which produced a RE of 19% and 17.3%, respectively, a significantly different from the values recorded for the individual-cv model (Tables 1 and 2).

Therefore, a general calibration model can be used for the prediction of $Anth_g$ in grape berries, with relative errors no higher than 14.1% and 19% for $ANTH_R$ and $ANTH_{RG}$, respectively, depending on both the cv and the growing site.

Fig. 2A and B show the scatter plots of the $Anth_g$ quantitative data and the $ANTH_R$ and $ANTH_{RG}$ indices, respectively, which were acquired during the 2010 campaign. The global calibration curve derived for $ANTH_R$ was still well represented ($R^2 = 0.932$) by a homographic function (Fig. 2A) with equation:

$$Anth_g = \frac{ANTH_R}{(1.5571 - 0.2832 ANTH_R)} \tag{3}$$

For the $ANTH_{RG}$ index, the data points were more dispersed (Fig. 2B) but still fairly ($R^2 = 0.797$) well fitted by a decaying exponential function, with equation:

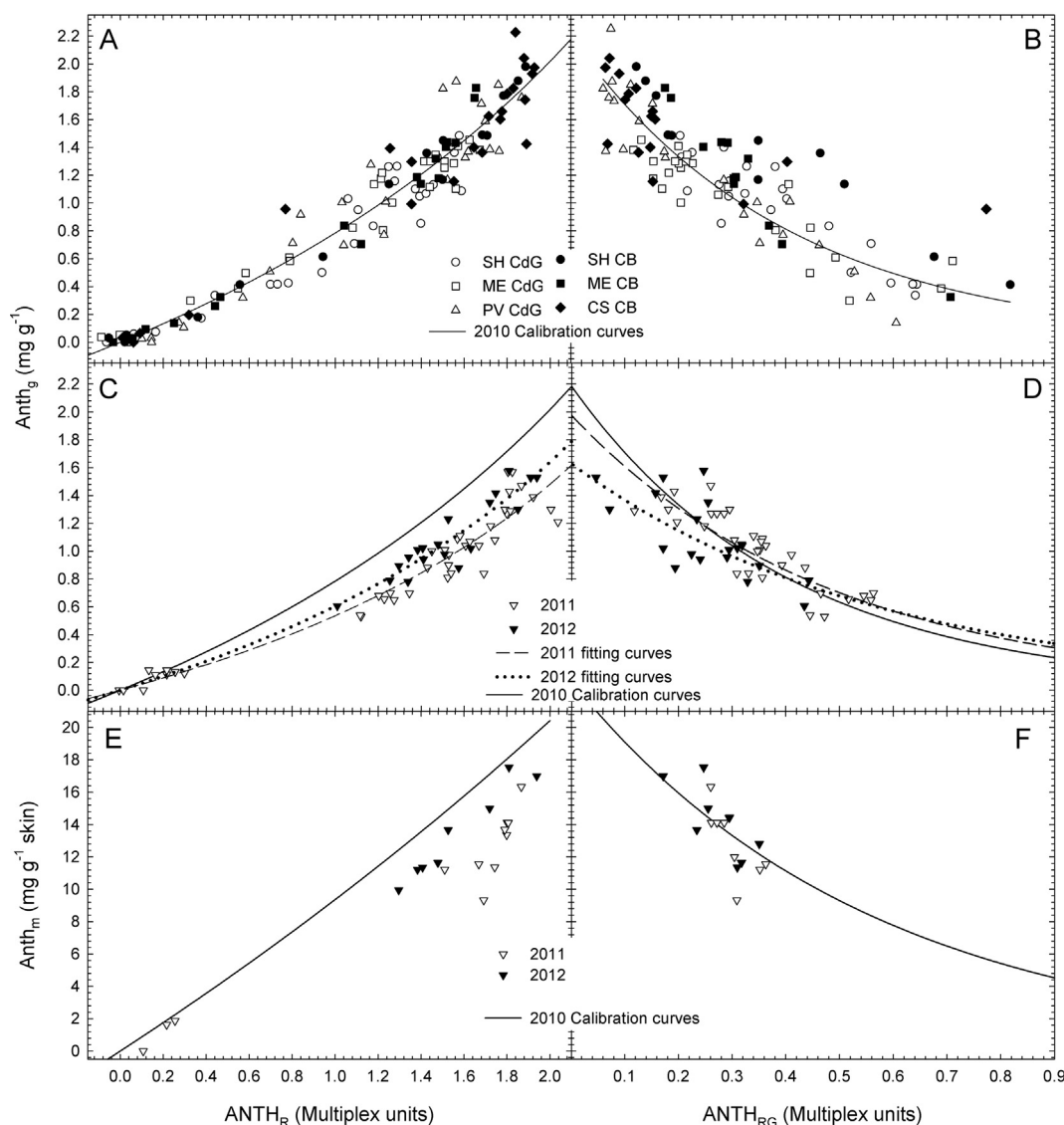$$Anth_g = 2.1924 e^{-2.4815 ANTH_{RG}} \tag{4}$$

Fig. 2. Global (inter-cultivar and inter-site) anthocyanin calibration curves for the Mx $ANTH_R$ (A) and $ANTH_{RG}$ (B) indices recorded in 2010. The homographic function in (A) has equation: $Anth_g = \frac{ANTH_R}{(1.5571 - 0.2832 ANTH_R)}$ ($R^2 = 0.932$). The exponential function in (B) has equation: $Anth_g = 2.1924 e^{-2.4815 ANTH_{RG}}$ ($R^2 = 0.797$). Comparison between the 2010 global curve and the 2011–2012 data sets for $ANTH_R$ (C) and $ANTH_{RG}$ (D) indices with the anthocyanin concentration reported on a berry mass basis ($Anth_g$). Comparison between the 2010 individual cultivar calibration curve for Shiraz (both sites) and the 2011–2012 data sets for $ANTH_R$ (E) and $ANTH_{RG}$ (F) indices with the anthocyanin concentration reported on a skin mass basis ($Anth_m$).

3.1.5. Seasonal effects

Seasonal robustness of the 2010 models was evaluated by plotting the calibration curves together with the data sets acquired in 2011 and 2012, as reported in Fig. 2C and D for $ANTH_R$ and $ANTH_{RG}$, respectively.

In considering $ANTH_R$, a significant shift in the data points, from véraison on, occurred among the seasons (Fig. 2C). As compared with 2010, the shift was greater for 2011 than for 2012. In considering $ANTH_{RG}$, the data sets of the three seasons were in agreement, even if the points for 2012 were rather dispersed, as can be seen in Fig. 2D.

Validation of the 2010 calibration curve on 2011 and 2012 data sets produced RMSEP for $ANTH_R$ of 0.4 and 0.31 mg g^{-1}, respectively, which corresponded to relative errors of 33% and 26%. For $ANTH_{RG}$, RMSEP was 0.21 and 0.26 mg g^{-1}, with relative errors of 17% and 22%, during the 2011 and 2012 seasons, respectively.

A conclusive explanation for this seasonal variability in the relationship between $Anth_g$ and the Mx Anth indices cannot be provided at present. One possible reason may "simply" be related to a way of expressing the Anth content in the berries that can affect its correlation with the non-destructive optical measurements. Since Anths are localized into the berry skin, using the skin mass based ($Anth_m$) or the berry mass based ($Anth_g$) concentrations can make a significant difference. To verify this aspect, the 2010 calibration curves were calculated again for the Mx indices by using $Anth_m$ and were newly analysed, in comparison with 2011 and 2012 data sets.

The conversion of $Anth_g$ to $Anth_m$ required a knowledge of the Relative Skin Mass (RSM), that is the skin mass to berry mass ratio, which was not available for our set of data. However, a simulation could be performed by considering the RSM values for specific cultivars found into the literature and using the formula $Anth_m = Anth_g/RSM$ to transform units. Within the Anth concentration conversion process, the previously reported changes in RSM during the growing season, from véraison to harvest, must be considered. In fact, according to Ojeda et al. (2002), the Shiraz RSM was calculated to vary from about 6% at pre-véraison to 9% at harvest, yet Keller and Hrazdina (1998) reported a change in RSM for Cabernet Sauvignon of between 8% and 10% within 6 weeks after véraison.

In Fig. 2E and F, the results of the simulation for the cv Shiraz, that considered data points from both the CdG and CB estates, are reported. For the $Anth_g$ to $Anth_m$ conversion, RSM values of 7% during véraison and 9% after véraison were applied.

The new 2010 calibration for both $ANTH_R$ and $ANTH_{RG}$ against $Anth_m$ in SH was similar to that against $Anth_g$, with homographic ($R^2 = 0.92$) and decaying exponential ($R^2 = 0.76$) fitting curves, respectively (to be compared with values in the second row, calibration column of Tables 1 and 2). Fig. 2E shows that the shift among data points of the three seasons concerning $ANTH_R$ remained, while the 2010 calibration curve for $ANTH_{RG}$ was well overlapped to the corresponding data points for 2011 and 2012 (Fig. 2F). Therefore, the seasonal effect on the calibration curves was substantially independent of the Anth concentration units.

Since RSM is significantly affected by the water stress and by the growing season, a simulation was performed of which change in RSM for Shiraz during the years of 2011 and 2012 could have had the best agreement with the 2010 calibration curve. Hence, for each index and year, the RMSEP was calculated as a function of the RSM, as reported in Fig. 3.

The minimum RMSEP for $ANTH_R$ (Fig. 3A) was registered for RSMs of 6.8% and 7.8% in 2011 and 2012, respectively. These values were lower than the 9% RSM assumed after véraison in 2010, an occurrence that is explainable by less favourable growing conditions for vines in 2010 and relative to 2011 and 2012. In fact, it was proved that when vine growth is reduced, there is an increase in the RSM of the berries (Cooley, Clingeleffer, & Walker, 2017; Ojeda et al., 2002; Roby, Harbertson, Adams, & Matthews, 2004).

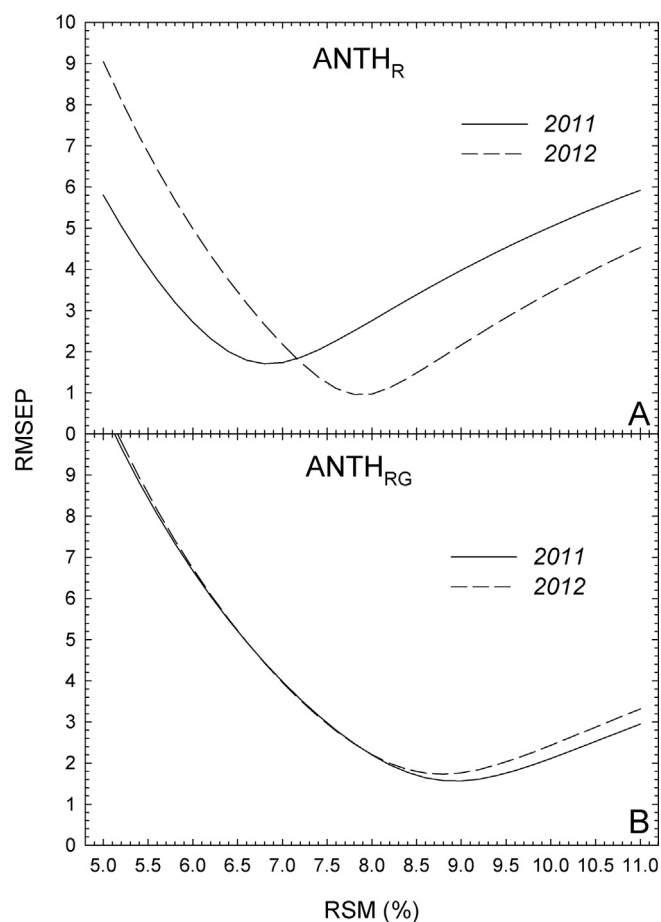Under water deficit RSM of Shiraz berries can reach values of more

Fig. 3. Root Mean Squared Error of Prediction (RMSEP) for the 2010 SH calibration curves (reported in Fig. 2E and F) validated over the 2011 and 2012 data sets as function of the berry Relative Skin Mass (RSM) for $ANTH_R$ (A) and $ANTH_{RG}$ (B).

than 10% (Ojeda et al., 2002). Roby et al. (2004) showed that, under low irrigation regimes, Cabernet Sauvignon berries had a RSM of 18% as compared with the 13% of the controls.

There is also a high inter-season variability of RSM (Palliotti, Gatti, & Poni, 2011). Bucchetti, Matthews, Falginella, Peterlunger, and Castellarin (2011) reported a variability in RSM from 9.6% to 12.1% at harvest in the cv Merlot between two consecutive seasons. Marked changes in RSM can also be induced by vine management practices that are used to control vine vigour, such as defoliation (Palliotti et al., 2011; Poni, Bernizzoni, Civardi, & Libelli, 2009).

For $ANTH_{RG}$ (Fig. 3B), the minimum RMSEP was obtained at similar RSM, 9% and 8.8% in 2011 and 2012, respectively, with no change compared with the 2010 values, which were considered from véraison to harvest. This result was in good agreement with the overlapping between the 2010 $ANTH_{RG}$ calibration curve and the data from the two following seasons shown in Fig. 2F.

To explain the seasonal effect on the calibration curves, we hypothesize that the different meteorological conditions for each year (see Fig. S1 and Table S1, Supplementary material) affect the berry RSM and this induced change has an effect on the $ANTH_R$ versus $Anth_m$ relationship.

Indeed, the growing degree days (GDD), representing the heat accumulation during the April–October period for 2010, was markedly lower than in 2011 and 2012 (1935 versus 2238 and 2316 at CB; 2247 versus 2350 and 2395 at CdG), and supported relatively higher RSM values in 2010 than in later years.

Finally, the $ANTH_{RG}$ index is less sensitive than $ANTH_R$ to the change in RSM, at least for the SH cultivar.

3.1.6. Closing remarks

The global model built with 2010 data from all cultivars at both sites can represent a valuable choice, thanks to the acceptable precision of prediction with maximal relative errors of about 14% and 19% for $ANTH_R$ and $ANTH_{RG}$, respectively. This precision is very close to that obtainable from the single-cultivar models (with RE $\leq 13.4\%$ and $\leq 16\%$ for $ANTH_R$ and $ANTH_{RG}$, respectively) and in some cases is even better, which suggests the possibility of applying the global model to an even wider range of cultivars and sites.

$ANTH_R$ calibration curves, both global and single-cultivar, were not stable with the years, with RE values of over 30%, apart from the SH case in 2012 (16.3%).

The constancy of the $ANTH_{RG}$ calibration curves over the years was satisfactory, with RE remaining around 20% in 2011–2012 for the global model. If we consider the single cultivar models, in 2011 and 2012 RE was 9.8% and 9.7%, respectively, for SH and 13.4% and 26.6%, respectively, for ME.

Possible causes of dispersion in the Anth versus ANTH relationship can be due to the light scattering from berry cell structures that may affect both the excitation and the emission signals of the sensor. This effect can be cv dependent and may affect differently $ANTH_R$ and $ANTH_{RG}$, due to the different transmittance properties of green and red light into the berry tissues.

Another possible contribution to the discrepancy between the in vitro and in vivo Anth determinations may be due to the absorbance properties of pigments in the in vivo environment, depending on pH, concentration and non-covalent binding of Anth to other molecules. These last reactions, determining the so-called Anth co-pigmentation, are well known processes occurring in wine (Boulton, 2001), however, no much information about their extent in the grape berry skin is available. Further studies are need to quantify the effects of these processes on the optical non-destructive Anth determination presented here.

3.2. In field applications

Here as follows are outlined some examples of applications of the calibrated Mx sensor for Anth quantitative estimates in the vineyard, such as i) a comparison of $Anth_g$ among different plots and years of the same cultivar per site; ii) a comparison of $Anth_g$ for the same cultivar between different sites and years; iii) a temporal evolution in $Anth_g$.

We used the $ANTH_{RG}$ prediction models for the in-field application of the sensor, because these are less susceptible to seasonal effects as compared with $ANTH_R$ ones (see Fig. 2C–F). The in-field calibration curves for $ANTH_{RG}$ were derived from the calibration curves built in the lab (see paragraph 2.5), by considering the overall data collected within the 3 seasons (2010, 2011 and 2012). The only exception was that of CS (2010 and 2011 data). All models were described by decaying exponential curves, with equations and parameters detailed in the following:

Global calibration curve (all cvs, both sites):

$$Anth_g = 2.9518\,e^{-4.9198ANTH_{RG}} \quad (R^2 = 0.787; RMSEC = 0.215\,mg\,g^{-1})$$

(5)

SH (single cv, both sites):

$$Anth_g = 3.5062\,e^{-5.2542ANTH_{RG}} \quad (R^2 = 0.860; RMSEC = 0.162\,mg\,g^{-1})$$

(6)

ME (single cv, both sites):

$$Anth_g = 2.6988\,e^{-4.6415ANTH_{RG}} \quad (R^2 = 0.726; RMSEC = 0.207\,mg\,g^{-1})$$

(7)

PV (single cv, CdG):

$$Anth_g = 3.1751\,e^{-5.9804ANTH_{RG}} \quad (R^2 = 0.870; RMSEC = 0.219\,mg\,g^{-1})$$

(8)

CS (single cv, CB):

$$Anth_g = 2.6127\,e^{-3.8054ANTH_{RG}} \quad (R^2 = 0.614; RMSEC = 0.211\,mg\,g^{-1})$$

(9)

These curves were applied in order to estimate $Anth_g$ from Mx data collected during the 2010 and 2011 campaigns. Values obtained from the global curve were compared with those from the single cv curves, and a difference in $Anth_g$ no greater than 18% was found.

It was below 10% in about 70% of cases out of a total of 32 plots analysed. Greater differences were observed only for SH of the CB winery (both years), SH of the CdG winery in 2010, and one plot of CS in 2011.

The global curve underestimated SH $Anth_g$ with no significant differences for CdG in 2011, but with significant differences in all the other cases (P ≤ 0.026).

ME $Anth_g$ was overestimated by the global curve, but at no more than 5%; moreover, only 3 cases out of 10 reported significant differences (data not shown).

Therefore, and as shown for the laboratory conditions, the choice of the global calibration curve appears to be adequate. However, the single-cultivar calibration can be adopted in the case of higher accuracy requirements for the Anth determination.

3.2.1. Anth content among different plots and years of the same cultivar per site

The $Anth_g$ content evaluated on different plots of the cultivars monitored over two consecutive campaigns (2010 and 2011) at the CdG and CB estates is reported in Fig. 4A–F. The number of bunches measured by the Mx sensor for each plot varied between 85 and 340, depending on the size of the plot. The $Anth_g$ content was calculated by using a single cultivar calibration curve and averaging Mx measurements taken at the moment of two temporal acquisitions, namely at harvest and one week previously. On the whole, as depicted in Fig. 4, one of the main advantages of using the sensor is to show differences among samples, even though there is an extensive variability. In general, more extensive sampling corresponds to a greater opportunity to see differences, even when these are very small.

ME at CdG was the most homogeneous cultivar among the plots considered (Fig. 4B).

$Anth_g$ of SH at CdG was constant among the plots in 2011, but not in 2010 (Fig. 4A). The opposite was observed for PV (Fig. 4C). For each of the three cvs investigated at CB, significant differences were always observed among the plots (Fig. 4D–F).

Variability in $Anth_g$ among plots of the same cv on a single growing site is a common feature. This may depend on the clones/rootstocks, the soil characteristics (Yokotsuka, Nagao, Nakazawa, & Sato, 1999), water (Deluc et al., 2009) and nutrient (Keller & Hrazdina, 1998) availability, and then on the vegetative status of the vines. An inverse relationship usually exists between grape Anth content and vine vigour (Cortell, Halbleib, Gallagher, Righetti, & Kennedy, 2007), this last showing a high spatial variability even within the same plot (Baluja et al., 2012b).

A significant difference between the two seasons was always registered with higher $Anth_g$ in 2010, except for plot 7 of PV at the CdG winery, even if at the limit of significance (P = 0.061). This result confirmed the less favourable growing conditions experienced by the vines in 2010 compared to 2011, as suggested by the comparison of GDD between the years (see Table S1 Supplementary material).

Extensive variations in grape Anth among the seasons have often been observed in other studies as being linked to the meteorological conditions (mainly to precipitation and to temperature) (Baluja, Tardaguila, Ayestaran, & Diago, 2013; Guidoni, Ferrandino, & Novello, 2008; Spayd, Tarara, Mee, & Ferguson, 2002).

3.2.2. Anth content for the same cultivar between different sites and years

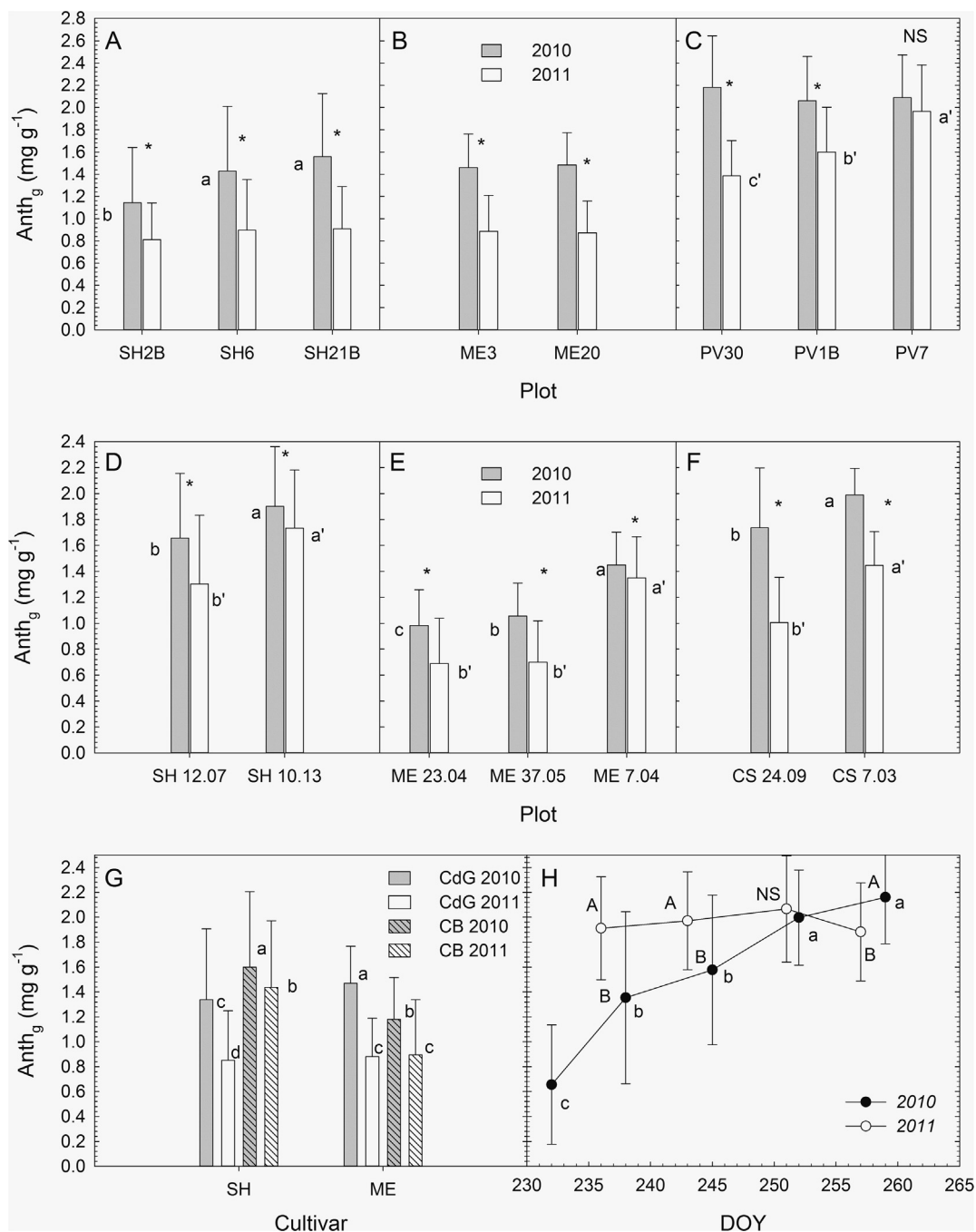The estimated $Anth_g$ averaged over several plots for the same

Fig. 4. Anth$_g$ content evaluated on different plots of the cultivars monitored over two consecutive campaigns (2010 and 2011) at the Casale del Giglio (CdG) estate: SH (A), ME (B) and PV (C), and at the Castello Banfi (CB) estate: SH (D), ME (E) and CS (F). Bars accompanied by asterisks indicate a significant difference (P < 0.001) between years for the same plot; different small letters (for 2010 campaign) and different small letters with apex (for 2011 campaign) mean significant different Anth$_g$ (P < 0.001). (G) Averaged estimated Anth$_g$ content in cultivars SH and ME from 2010 and 2011 campaigns at CdG and CB wineries. Bars accompanied by different small letters indicate significant different Anth$_g$ (P < 0.001). (H) Temporal evolution of Anth content in cv PV (plot PV7) during the 2010 and 2011 seasons. Points with different capital letters indicate a significant difference (P < 0.001) between years for the similar collecting date; different small letters mean a significant difference (P < 0.001) among DOY (occurring only in 2010).

cultivar (SH or ME) at each location in the proximity of the harvest in 2010 and 2011 are compared in Fig. 4G. In this case, the number of bunches sampled by the Mx for each determination increased, and ranged from 216 (ME at CdG in 2011) to 717 (ME at CB in 2011).

SH was the most heterogeneous cultivar, being characterized by significant differences between seasons and sites. The Anth$_g$ was higher at CB than at CdG for both years. The average value of Anth$_g$ content in ME plots differed significantly between the wineries in 2010, but not during the 2011 season. Again, this fluctuation can be ascribed to the combination of differences on the two sites in clone characteristics, soil

texture, climatic conditions and cultural practices (Guidoni et al., 2008; Poni et al., 2009). Generally speaking, in 2010 the Anth$_g$ accumulation was larger than it was during the 2011 season.

3.2.3. Temporal evolution of Anth content

The temporal evolution of Anth content in the cv PV (plot 7) during the 2010 and 2011 campaigns is reported in Fig. 4H, where each point represents the average of 20–45 bunches.

In 2010, the accumulation of Anth was delayed as compared with 2011, and increased significantly from DOY 232 to harvest (DOY 259).

In 2011, $Anth_g$ had already reached a plateau (1.9–2.0 mg g^{-1}) at the beginning of the monitoring (DOY 236), and remained constant for 2 weeks. After that, a tendency to decrease appeared even if it was not statistically significant. The 2010 $Anth_g$ exceeded the 2011 value at harvest time. The kinetics recorded clearly showed the seasonal climatic differential effect on the synthesis of Anth.

4. Conclusions

In this paper, the Mx fluorescence sensor, widely used as a tool in viticulture, has been calibrated against chemical determinations of the grape Anth. The destructive analysis was focused on the measurement of the total berry skin Anth, the so-called total potential in anthocyanins of grapes, by using low pH extraction. This represent the amount that is expected to better correlate with the in vivo determinations provided by the Mx sensor.

To predict wine colour, oenologist would appreciate considering also the Anth extractability, measured by using berry extraction at pH 3.2, to simulate the fermentation condition. Calibration of the sensor against the extractable anthocyanin fraction was out of the scope of the present paper and could be evaluated in a future work. However, the additional variability in the extractability due to its dependence on cultivars and winemaking techniques can make the utility of this calibration questionable. On the other hand, good correlations between total anthocyanins in the grape and those found into the derived wine are often reported into the literature (Fragoso, Guasch, Aceña, Mestres, & Busto, 2011; González-Neves et al., 2004; Ristic, Bindon, Francis, Herderich, & Iland, 2010).

The completeness of the analytical approach presented herein is supported by the use of data from four cultivars, two geographical areas, and three consecutive years of production, in order to guarantee the highest repeatability and reproducibility.

The main results concern: 1) the definition of a very general global calibration curve essentially similar, in Anth prediction, to single-cultivar curves and rather independent of grape cultivar and growing site; 2) proof of the seasonal robustness of the $ANTH_{RG}$ calibration curves, as well as of the seasonal susceptibility of $ANTH_R$ calibration curves due to climatic changes in the berry morphology (Relative Skin Mass); 3) the demonstration of the practical utility of a fluorescence sensor for precision viticulture purposes.

Thanks to the massive sampling performed in the vineyards by the optical sensor, it was possible to show differences in Anth among plots, despite an extensive biological variability. Acquisition of these online data can be useful for making decisions on the best harvest time or for better defining the vine management. Mapping large plots by means of the Mx proximal sensing is also possible in order to perform selective harvesting and to produce wines with a differentiated quality. The information provided by the Mx sensor on total Anth through the prediction models developed here can then be helpful for both viticulturists and oenologists.

Acknowledgements

Conflict of interest

None.

Appendix A. Supplementary data

Supplementary data associated with this article can be found, in the online version, at http://dx.doi.org/10.1016/j.foodchem.2017.10.021.

References

Agati, G., D'Onofrio, C., Ducci, E., Cuzzola, A., Remorini, D., Tuccio, L., ... Mattii, G. (2013). Potential of a multiparametric optical sensor for determining in situ maturity components of red and white *Vitis vinifera* wine grapes. *Journal of Agricultural and Food Chemistry, 61*, 12211–12218.

Agati, G., Meyer, S., Matteini, P., & Cerovic, Z. G. (2007). Assessment of Anthocyanins in Grape (*Vitis vinifera* L.) berries using a noninvasive chlorophyll fluorescence method. *Journal of Agricultural and Food Chemistry, 55*, 1053–1061.

Baluja, J., Diago, M. P., Goovaerts, P., & Tardaguila, J. (2012a). Spatio-temporal dynamics of grape anthocyanin accumulation in a Tempranillo vineyard monitored by proximal sensing. *Australian Journal of Grape and Wine Research*. http://dx.doi.org/10.1111/j.1755-0238.2012.00186.x, 173-182.

Baluja, J., Diago, M. P., Goovaerts, P., & Tardaguila, J. (2012b). Assessment of the spatial variability of anthocyanins in grapes using a fluorescence sensor: relationships with vine vigour and yield. *Precision Agriculture*. http://dx.doi.org/10.1007/s11119-012-9261-x.

Baluja, J., Tardaguila, J., Ayestaran, B., & Diago, M. P. (2013). Spatial variability of grape composition in a Tempranillo (*Vitis vinifera* L.) vineyard over a 3-year survey. *Precision Agriculture, 14*(1), 40–58.

Ben Ghozlen, N., Cerovic, Z. G., Germain, C., Toutain, S., & Latouche, G. (2010). Non-destructive optical monitoring of grape maturation by proximal sensing. *Sensors, 10*, 10040–10068.

Boss, P. K., Davies, C., & Robinson, S. P. (1996). Analysis of the expression of anthocyanin pathway genes in developing *Vitis vinifera* L. cv. Shiraz grape berries and the implications for pathway regulation. *Plant Physiology, 111*, 1059–1066.

Boulton, R. (2001). The copigmentation of anthocyanins and its role in the color of red wine: a critical review. *American Journal of Enology and Viticulture, 52*(2), 67–87.

Bramley, R. G. V., Le Moigne, M., Evain, S., Ouzman, J., Florin, L., Fadaili, E. M., ... Cerovic, Z. G. (2011). On-the-go sensing of grape berry anthocyanins during commercial harvest: development and prospects. *Australian Journal of Grape and Wine Research, 17*, 316–326.

Bucchetti, B., Matthews, M. A., Falginella, L., Peterlunger, E., & Castellarin, S. D. (2011). Effect of water deficit on Merlot grape tannins and anthocyanins across four seasons. *Scientia Horticulturae, 128*, 297–305.

Cerovic, Z. G., Latouche, G., Nguyen, H. K., Fadaili, E. M., Le Moigne, M., & Ben Ghozlen, N. (2014). CUBA: An internet-based software application for berry anthocyanins units' conversion for viticulturists, oenologists and physiologists. *Computers and Electronics in Agriculture, 103*, 122–126.

Cerovic, Z. G., Moise, N., Agati, G., Latouche, G., Ben Ghozlen, N., & Meyer, S. (2008). New portable optical sensors for the assessment of winegrape phenolic maturity based on berry fluorescence. *Journal of Food Composition and Analysis, 21*, 650–654.

Chen, S., Zhang, F., Ning, J., Liu, X., Zhang, Z., & Yang, S. (2015). Predicting the anthocyanin content of wine grapes by NIR hyperspectral imaging. *Food Chemistry, 172*, 788–793.

Cooley, N. M., Clingeleffer, P. R., & Walker, R. R. (2017). Effect of water deficits and season on berry development and composition of Cabernet Sauvignon (*Vitis vinifera* L.) grown in a hot climate. *Australian Journal of Grape and Wine Research, 23*(2), 260–272.

Cortell, J. M., Halbleib, M., Gallagher, A. V., Righetti, T. L., & Kennedy, J. A. (2007). Influence of vine vigor on grape (*Vitis vinifera* L. cv. Pinot Noir) anthocyanins. 1. Anthocyanin concentration and composition in fruit. *Journal of Agricultural and Food Chemistry, 55*(16), 6575–6584.

Deluc, L. G., Quilici, D. R., Decendit, A., Grimplet, J., Wheatley, M. D., Schlauch, K. A., ... Cramer, G. R. (2009). Water deficit alters differentially metabolic pathways affecting important flavor and quality traits in grape berries of Cabernet Sauvignon and Chardonnay. *BMC Genomics, 10*, 212–245.

Diago, M. P., Rey-Carames, C., Le Moigne, M., Fadaili, E. M., Tardaguila, J., & Cerovic, Z. G. (2016). Calibration of non-invasive fluorescence-based sensors for the manual and on-the-go assessment of grapevine vegetative status in the field. *Australian Journal of Grape and Wine Research, 22*, 438–449.

Ferrandino, A., Pagliarani, C., Carlomagno, A., Novello, V., Schubert, A., & Agati, G. (2017). Improved fluorescence-based evaluation of flavonoid in red and white wine grape cultivars. *Australian Journal of Grape and Wine Research, 23*, 207–214.

Fragoso, S., Guasch, J., Aceña, L., Mestres, M., & Busto, O. (2011). Prediction of red wine colour and phenolic parameters from the analysis of its grape extract. *International Journal of Food Science & Technology, 46*(12), 2569–2575.

González-Neves, G., Charamelo, D., Balado, J., Barreiro, L., Bochicchio, R., Gatto, G., et al. (2004). Phenolic potential of Tannat, Cabernet-Sauvignon and Merlot grapes and their correspondence with wine composition. *Analytica Chimica Acta, 513*(1), 191–196.

Guidoni, S., Ferrandino, A., & Novello, V. (2008). Effects of seasonal and agronomical practices on skin anthocyanin profile of Nebbiolo grapes. *American Journal of Enology and Viticulture, 59*(1), 22–29.

Keller, M., & Hrazdina, G. (1998). Interaction of nitrogen availability during bloom and light intensity during veraison. II. Effects on anthocyanin and phenolic development during grape ripening. *American Journal of Enology and Viticulture, 49*(3), 341–349.

Kennedy, J. A., Matthews, M. A., & Waterhouse, A. L. (2002). Effect of maturity and vine water status on grape skin and wine flavonoids. *American Journal of Enology and*

Viticulture, 53, 268–274.

Nogales-Bueno, J., Baca-Bocanegra, B., Rodríguez-Pulido, F. J., Heredia, F. J., & Hernández-Hierro, J. M. (2015). Use of near infrared hyperspectral tools for the screening of extractable polyphenols in red grape skins. *Food Chemistry, 172*, 559–564.

Ojeda, H., Andary, C., Kraeva, E., Carbonneau, A., & Deloire, A. (2002). Influence of pre- and postveraison water deficit on synthesis and concentration of skin phenolic compounds during berry growth of Vitis vinifera cv. Shiraz. *American Journal of Enology and Viticulture, 53*(4), 261–267.

Palliotti, A., Gatti, M., & Poni, S. (2011). Early leaf removal to improve vineyard efficiency: gas exchange, source-to-sink balance, and reserve storage responses. *American Journal of Enology and Viticulture, 62*(2), 219–228.

Poni, S., Bernizzoni, F., Civardi, S., & Libelli, N. (2009). Effects of pre-bloom leaf removal on growth of berry tissues and must composition in two red *Vitis vinifera* L. cultivars. *Australian Journal of Grape and Wine Research, 15*(2), 185–193.

Ristic, R., Bindon, K., Francis, L. I., Herderich, M. J., & Iland, P. G. (2010). Flavonoids and C13-norisoprenoids in Vitis vinifera L. cv. Shiraz: relationships between grape and wine composition, wine colour and wine sensory properties. *Australian Journal of Grape and Wine Research, 16*(3), 369–388.

Roby, G., Harbertson, J. F., Adams, D. A., & Matthews, M. A. (2004). Berry size and vine water deficits as factors in winegrape composition: anthocyanins and tannins. *Australian Journal of Grape and Wine Research, 10*(2), 100–107.

Spayd, S. E., Tarara, J. M., Mee, D. L., & Ferguson, J. C. (2002). Separation of sunlight and temperature effects on the composition of *Vitis vinifera* cv. Merlot berries. *American Journal of Enology and Viticulture, 53*(3), 171–182.

Tuccio, L., Remorini, D., Pinelli, P., Fierini, E., Tonutti, P., Scalabrelli, G., & Agati, G. (2011). Rapid and non-destructive method to assess in the vineyard grape berry anthocyanins under different seasonal and water conditions. *Australian Journal of Grape and Wine Research, 17*, 181–189.

Winkler, A. J. (1974). *General viticulture*. Univ of California Press.

Yokotsuka, K., Nagao, A., Nakazawa, K., & Sato, M. (1999). Changes in anthocyanins in berry skins of Merlot and Cabernet Sauvignon grapes grown in two soils modified with limestone or oyster shell versus a native soil over two years. *American Journal of Enology and Viticulture, 50*(1), 1–12.

Zhang, N., Liu, X., Jin, X., Li, C., Wu, X., Yang, S., ... Yanne, P. (2017). Determination of total iron-reactive phenolics, anthocyanins and tannins in wine grapes of skins and seeds based on near-infrared hyperspectral imaging. *Food Chemistry, 237*(2017), 811–817.